Article

Cell Metabolism

SLC39A14 Is Required for the Development of Hepatocellular Iron Overload in Murine Models of Hereditary Hemochromatosis

Graphical Abstract

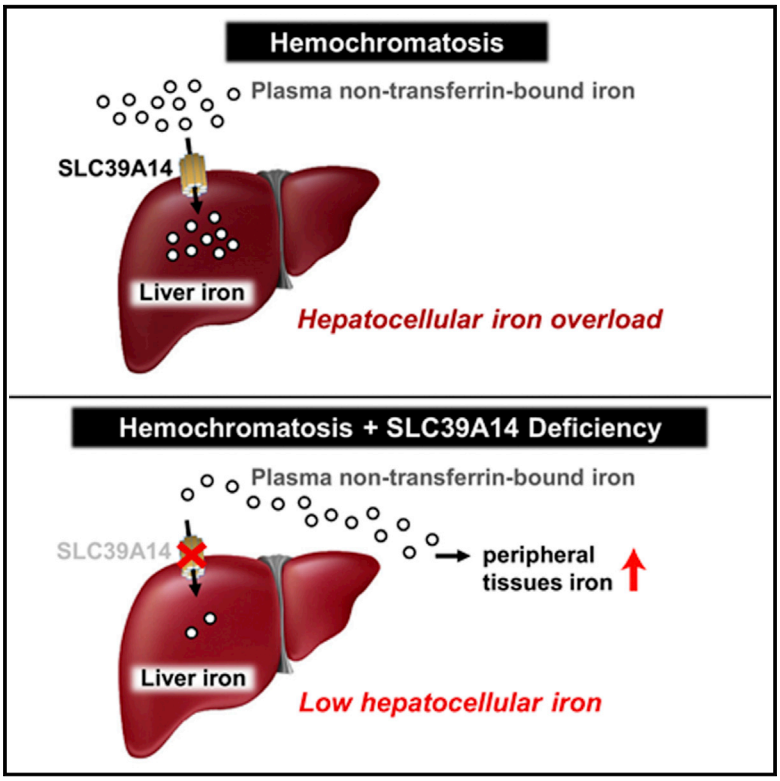

Authors

Supak Jenkitkasemwong, Chia-Yu Wang, Richard Coffey, ..., Shintaro Hojyo, Toshiyuki Fukada, Mitchell D. Knutson

Correspondence

mknutson@ufl.edu

In Brief

Plasma non-transferrin-bound iron (NTBI) is a main contributor to tissue iron loading in iron overload disorders such as hereditary hemochromatosis. Jenkitkasemwong et al. show that loss of the metal-ion transporter SLC39A14 impairs NTBI uptake by the liver and prevents hepatic iron overload in mouse models of hemochromatosis.

Highlights

- SLC39A14 mediates non-transferrin-bound iron uptake by the liver and pancreas
- SLC39A14 is required for *Hfe*$^{-/-}$ and *Hfe2*$^{-/-}$ mice to develop hepatic iron overload
- SLC39A14 is required for iron loading of hepatocytes and pancreatic acinar cells
- SLC39A14 represents a possible therapeutic target for mitigating tissue iron loading

Jenkitkasemwong et al., 2015, Cell Metabolism *22*, 138–150
July 7, 2015
http://dx.doi.org/10.1016/j.cmet.2015.05.002

CellPress

Cell Metabolism
Article

SLC39A14 Is Required for the Development of Hepatocellular Iron Overload in Murine Models of Hereditary Hemochromatosis

Supak Jenkitkasemwong,[1] Chia-Yu Wang,[1] Richard Coffey,[1] Wei Zhang,[1] Alan Chan,[1] Thomas Biel,[2] Jae-Sung Kim,[2] Shintaro Hojyo,[3,4] Toshiyuki Fukada,[3,5,6] and Mitchell D. Knutson[1,*]
[1]Food Science and Human Nutrition Department
[2]Department of Surgery
University of Florida, Gainesville, FL 32611, USA
[3]RIKEN Center for Integrative Medical Sciences, Yokohama 230-0045, Japan
[4]Deutsches Rheuma-Forschungszentrum Berlin, Osteoimmunology, Charitéplatz, 10117 Berlin, Germany
[5]Division of Pathology, Department of Oral Diagnostic Sciences, School of Dentistry, Showa University, Shinagawa 142-8666, Japan
[6]Molecular and Cellular Physiology, Faculty of Pharmaceutical Sciences, Tokushima Bunri University, Tokushima 770-8055, Japan
*Correspondence: mknutson@ufl.edu
http://dx.doi.org/10.1016/j.cmet.2015.05.002

SUMMARY

Nearly all forms of hereditary hemochromatosis are characterized by pathological iron accumulation in the liver, pancreas, and heart. These tissues preferentially load iron because they take up non-transferrin-bound iron (NTBI), which appears in the plasma during iron overload. Yet, how tissues take up NTBI is largely unknown. We report that ablation of *Slc39a14*, the gene coding for solute carrier SLC39A14 (also called ZIP14), in mice markedly reduced the uptake of plasma NTBI by the liver and pancreas. To test the role of SLC39A14 in tissue iron loading, we crossed *Slc39a14*$^{-/-}$ mice with *Hfe*$^{-/-}$ and *Hfe2*$^{-/-}$ mice, animal models of type 1 and type 2 (juvenile) hemochromatosis, respectively. *Slc39a14* deficiency in hemochromatotic mice greatly diminished iron loading of the liver and prevented iron deposition in hepatocytes and pancreatic acinar cells. The data suggest that inhibition of SLC39A14 may mitigate hepatic and pancreatic iron loading and associated pathologies in iron overload disorders.

INTRODUCTION

Hereditary hemochromatosis is an autosomal recessive disorder that results from increased intestinal iron absorption and subsequent iron accumulation in body tissues. More than 80% of cases of hereditary hemochromatosis arise from a C282Y mutation in the *HFE* gene (Feder et al., 1996). With a carrier frequency of 1:200 to 1:300, the C282Y mutation is one of the most prevalent polymorphisms in individuals of northern European descent (Merryweather-Clarke et al., 1997). In *HFE*-related (type 1) hemochromatosis (OMIM 235200), iron absorption is increased because of inadequate synthesis of hepcidin (Bridle et al., 2003), the iron-regulatory hormone that limits iron absorption when body iron stores increase (Ganz and Nemeth, 2011). Accordingly, mutations in other genes required for hepcidin synthesis also lead to hereditary hemochromatosis. These genes include *HFE2*, commonly known as hemojuvelin (Papanikolaou et al., 2004); *HAMP*, the hepcidin gene (Roetto et al., 2003); and *TFR2*, transferrin receptor 2 (Camaschella et al., 2000). Mutations in *HFE2* and *HAMP* result in early-onset and severe iron overload, clinically referred to as juvenile (type 2) hemochromatosis (OMIM 602390). In hemochromatosis, iron loads primarily in the liver starting with periportal hepatocytes (Pietrangelo, 2010). As the disease progresses, iron accumulates in the remainder of the liver and also in the pancreas, where it deposits predominantly in acinar cells (Rahier et al., 1987). Later in the disease, iron loads in the myocardium of the heart (Carpenter et al., 2013). Clinical manifestations of hereditary hemochromatosis include hepatic fibrosis, cirrhosis, diabetes, and cardiomyopathy (Pietrangelo, 2010).

Hepcidin deficiency results in not only increased iron absorption but also increased iron release from reticuloendothelial macrophages of the liver, spleen, and bone marrow that recycle iron from senescent red blood cells (Knutson and Wessling-Resnick, 2003). Such unregulated iron entry into the plasma leads to increased saturation of transferrin, the plasma protein that transports iron. High plasma transferrin saturations, typically >75% in hereditary hemochromatosis, are associated with the presence of a redox-active, chelatable pool of iron known as "non-transferrin-bound iron" (NTBI) (Le Lan et al., 2005). First described in thalassemia major patients in 1978 (Hershko et al., 1978), NTBI is now widely believed to be a major contributor to tissue iron loading and related pathologies in iron overload disorders (Brissot et al., 2012; Cabantchik, 2014; Fleming et al., 2005). Studies in mice have demonstrated that NTBI in the plasma is rapidly and efficiently taken up mostly by the liver and, to a lesser extent, the pancreas, kidney, and heart (Bradbury et al., 1994; Craven et al., 1987; Wang and Knutson, 2013).

Despite the importance of NTBI in the pathophysiology of iron overload, the molecular mechanisms responsible for its tissue uptake have remained elusive (Brissot et al., 2012). The most

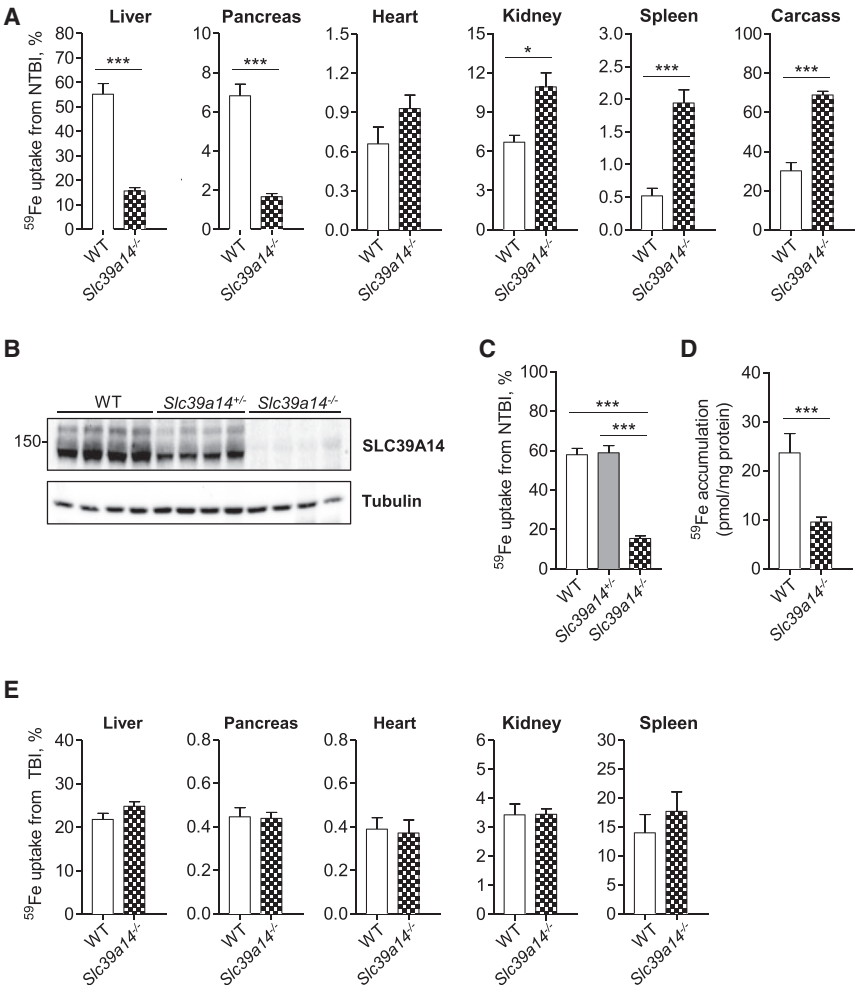

Figure 1. Hepatic and Pancreatic Uptake of Intravenously Administered ^{59}Fe-NTBI Is Impaired in *Slc39a14*$^{-/-}$ Mice

(A) In vivo ^{59}Fe-NTBI uptake by various tissues of 6-week-old wild-type (WT, n = 5) and *Slc39a14*$^{-/-}$ mice (n = 10). Tissue uptake of ^{59}Fe from NTBI was calculated as a percentage of whole-body cpm.

(B) Immunoblot analysis of SLC39A14 in liver homogenates from WT, *Slc39a14*$^{+/-}$, and *Slc39a14*$^{-/-}$ mice (n = 4 per group).

(C) In vivo ^{59}Fe-NTBI uptake by the liver in WT (n = 10), *Slc39a14*$^{+/-}$ (n = 9), and *Slc39a14*$^{-/-}$ (n = 15) mice.

(D) In vitro ^{59}Fe-NTBI uptake by cultures of primary hepatocytes isolated from 13-week-old WT and *Slc39a14*$^{-/-}$ mice. Data are presented as pmol ^{59}Fe per mg of protein (n = 3 per group).

(E) In vivo ^{59}Fe-TBI uptake by various tissues of 6-week-old WT and *Slc39a14*$^{-/-}$ mice (n = 4–5 per group). Tissue uptake of ^{59}Fe from TBI was calculated as a percentage of whole-body cpm. Data are presented as percent of total body cpm. Significance was calculated by using Student's t test. All data are shown as the mean ± SEM. ***p < 0.001, *p < 0.05.

frequently proposed candidate for mediating NTBI uptake has been divalent metal-ion transporter-1, DMT1 (SLC11A2), which is required for intestinal uptake of dietary iron and iron uptake by developing erythroid cells (Gunshin et al., 2005). We recently tested the hypothesis that DMT1 plays a role in hepatic NTBI uptake by using liver-specific *Dmt1* knockout mice and found that it is dispensable for hepatic NTBI uptake and hepatocyte iron loading (Wang and Knutson, 2013). A more recent candidate for NTBI uptake is SLC39A14, a member of the ZIP family of metal-ion transporters, which have mainly been characterized by their ability to transport zinc (Taylor et al., 2005). In 2006, we discovered that SLC39A14 could transport iron in addition to zinc, and that it mediated NTBI uptake by cultured AML12 mouse hepatocytes (Liuzzi et al., 2006). Subsequently, we demonstrated that SLC39A14 also mediated NTBI uptake in human hepatoma cells (Gao et al., 2008) and that the iron transport properties of SLC39A14, when expressed in *Xenopus laevis* oocytes, were consistent with studies of hepatic NTBI uptake in vivo (Pinilla-Tenas et al., 2011). Among human tissues, SLC39A14 is most abundantly expressed in liver, pancreas, and heart (Nomura et al., 1994; Taylor et al., 2005; Wang et al., 2012), suggesting that it may contribute to NTBI uptake and iron accumulation by these tissues in iron overload disorders.

Consistent with a possible role for SLC39A14 in NTBI uptake by the liver and pancreas is our observation that SLC39A14 protein levels are elevated in iron-loaded liver and pancreas (Nam et al., 2013). Here we formally tested the role of SLC39A14 in tissue NTBI uptake and iron loading by using *Slc39a14*$^{-/-}$ mice (Hojyo et al., 2011), double-knockout *Hfe*$^{-/-}$;*Slc39a14*$^{-/-}$ and *Hfe2*$^{-/-}$;*Slc39a14*$^{-/-}$ mouse models of hereditary hemochromatosis, and *Slc39a14*$^{-/-}$ mice subjected to dietary iron overload. We show that SLC39A14 is the main NTBI transporter in the liver and pancreas, that it is essential for the development of hepatic iron overload in hemochromatosis, and that it is required for iron loading of hepatocytes and pancreatic acinar cells.

RESULTS

Ablation of *Slc39a14* Impairs NTBI Uptake

To test the hypothesis that SLC39A14 plays a role in NTBI uptake in vivo, we used *Slc39a14*$^{-/-}$ mice and wild-type (WT) mice at 6 weeks of age. Mice were given an intravenous injection of ferric citrate to transiently saturate plasma transferrin, followed by an intravenous injection of ^{59}Fe-labeled ferric citrate representing NTBI. Two hours later, mice were sacrificed and tissues were harvested for gamma counting. We found that ^{59}Fe-NTBI uptake was 70% lower in the liver and pancreas of *Slc39a14*$^{-/-}$ mice compared with WT mice (Figure 1A). By contrast, ^{59}Fe-NTBI uptake by the kidney, spleen, and carcass was higher in *Slc39a14*$^{-/-}$ mice compared with WT controls. Analysis of hepatic ^{59}Fe-NTBI uptake from heterozygous animals, which expressed ~50% of WT SLC39A14 protein levels (Figure 1B),

indicates that one allele of *Slc39a14* is sufficient for normal hepatic NTBI clearance (Figure 1C). Immunoblot analyses confirmed the lack of SLC39A14 protein in *Slc39a14*$^{-/-}$ mouse liver (Figure 1B), pancreas, heart (Nam et al., 2013), and kidney (data not shown). To investigate whether the impaired hepatic NTBI uptake in *Slc39a14*$^{-/-}$ mice is due to a defect in uptake by hepatocytes, where SLC39A14 protein is most abundantly expressed in the liver (Nam et al., 2013), we measured ^{59}Fe-NTBI uptake in isolated primary hepatocytes. Similar to the liver, hepatocyte NTBI uptake from *Slc39a14*$^{-/-}$ mice was markedly impaired (Figure 1D).

We previously reported that SLC39A14 promotes the assimilation of transferrin-bound iron (TBI) by cultured cells (Zhao et al., 2010). Given that plasma TBI delivers iron to nearly all cells and may contribute to iron loading of the liver (Trinder and Morgan, 1997) and perhaps other tissues, we assessed whether tissue uptake of TBI is affected in *Slc39a14*$^{-/-}$ mice. We found that ^{59}Fe uptake from TBI was not altered in the liver, pancreas, heart, kidney, and spleen of *Slc39a14*$^{-/-}$ mice (Figure 1E), indicating that SLC39A14 is dispensable for TBI uptake in these tissues.

Loss of *Slc39a14* Prevents Hepatic Iron Overload in Hemochromatosis

To determine whether SLC39A14 is required for tissue iron accumulation in iron overload, we crossed *Slc39a14*$^{-/-}$ mice with *Hfe*$^{-/-}$ mice, the animal model of *HFE*-related hereditary hemochromatosis, to generate double-knockout *Hfe*$^{-/-}$;*Slc39a14*$^{-/-}$ mice. Similar to patients with the C282Y mutation in *HFE*, *Hfe*$^{-/-}$ mice hyperabsorb dietary iron and deposit it primarily in the liver (Zhou et al., 1998). Accordingly, we found that *Hfe*$^{-/-}$ mice at 4 weeks of age displayed elevated concentrations of non-heme iron, an indicator of iron stores, in the liver, but not the pancreas, heart, kidney, or spleen (Figure 2A). By contrast, *Hfe*$^{-/-}$;*Slc39a14*$^{-/-}$ mice did not accumulate iron in the liver, but did load iron in the kidney. The lack of hepatic iron accumulation in *Hfe*$^{-/-}$;*Slc39a14*$^{-/-}$ mice was associated not with impaired dietary iron absorption (Figure 2B) but instead with impaired hepatic iron accumulation of absorbed iron (Figure 2C). Although iron absorption did not differ significantly among groups (Figure 2B), two-way ANOVA revealed a significant main effect of genotype, with mice lacking *Hfe* having significantly higher iron absorption ($p < 0.05$). Histochemical staining for ferric iron deposits (Perls' stain) in liver sections from *Hfe*$^{-/-}$ mice revealed a periportal distribution of iron (Figure 2D), consistent with previous studies (Fleming et al., 2001; Zhou et al., 1998). In *Hfe*$^{-/-}$;*Slc39a14*$^{-/-}$ mice, negligible amounts of iron were detectable by using Perls' stain (Figure 2E) or the more sensitive DAB-enhanced Perls' stain (Figure 2F). Given that the liver can take up iron from the plasma, we measured plasma iron concentrations, total iron-binding capacity (TIBC), transferrin saturation, and plasma concentrations of NTBI (Figures 2G–2J). Plasma iron indices were not significantly affected by loss of *Slc39a14*, indicating that the lack of hepatic iron accumulation in *Hfe*$^{-/-}$;*Slc39a14*$^{-/-}$ mice is not due to diminished levels of plasma iron. As in our previous study (Hojyo et al., 2011), body weights of 4-week-old *Slc39a14*$^{-/-}$ mice were lower than those of WT mice (Figure 2K). Body weights of *Hfe*$^{-/-}$;*Slc39a14*$^{-/-}$ mice tended to be lower than those of WT or *Hfe*$^{-/-}$ mice, but the difference was not statistically significant. Tissue nonheme iron concentrations were also assessed at 16 weeks of age (see Figure S1D online). Similar to 4-week-old mice, 16-week-old *Hfe*$^{-/-}$;*Slc39a14*$^{-/-}$ mice displayed a marked impairment in hepatic iron accumulation and enhanced iron accumulation in the kidney. In addition, nonheme iron concentrations in the pancreas and heart were 60% and 24% higher, respectively, in *Hfe*$^{-/-}$;*Slc39a14*$^{-/-}$ mice compared to *Slc39a14*$^{-/-}$ animals.

To determine what effect a loss of *Slc39a14* would have in a more severe form of hemochromatosis, we generated double-knockout *Hfe2*$^{-/-}$;*Slc39a14*$^{-/-}$ mice. *Hfe2*$^{-/-}$ mice, the animal model for juvenile hemochromatosis, develop rapid and massive iron overload, with iron depositing primarily in the liver and secondarily in the pancreas and heart (Niederkofler et al., 2005). *Hfe2*$^{-/-}$ mice at 6 weeks of age exhibited elevated iron content of the liver (~15-fold), pancreas (~17-fold), and heart (~1-fold) compared with WT controls (Figure 3A). Similar to *Hfe*$^{-/-}$;*Slc39a14*$^{-/-}$ mice, double-knockout *Hfe2*$^{-/-}$;*Slc39a14*$^{-/-}$ mice displayed a marked impairment in iron loading of the liver (Figure 3A). In addition, iron loading of the pancreas was 60% less in *Hfe2*$^{-/-}$;*Slc39a14*$^{-/-}$ mice compared with *Hfe2*$^{-/-}$ controls. Interestingly, in comparison with *Hfe2*$^{-/-}$ animals, *Hfe2*$^{-/-}$;*Slc39a14*$^{-/-}$ mice displayed 26% higher nonheme iron concentrations in the heart and markedly elevated iron concentrations in the kidney and spleen (2.6- and 11-fold, respectively). These observations demonstrate that the heart, kidney, and spleen have SLC39A14-independent pathways of iron accumulation.

As expected, iron absorption was markedly elevated in *Hfe2*$^{-/-}$ mice (Figure 3B). Iron absorption was also elevated in *Hfe2*$^{-/-}$;*Slc39a14*$^{-/-}$ mice compared to WT or *Slc39a14*$^{-/-}$ animals but was 25% lower than in *Hfe2*$^{-/-}$ mice. The lower iron absorption in *Hfe2*$^{-/-}$;*Slc39a14*$^{-/-}$ mice was not associated with differences in enterocyte protein levels of DMT1, the apical iron importer, or ferroportin (FPN), the basolateral iron exporter (Figure S2). Similar to *Hfe*$^{-/-}$;*Slc39a14*$^{-/-}$ mice (Figure 2C), *Hfe2*$^{-/-}$;*Slc39a14*$^{-/-}$ mice showed diminished hepatic accumulation of absorbed iron compared with *Hfe2*$^{-/-}$ animals (Figure 3C). A trend of enhanced uptake of absorbed iron into the pancreas of *Hfe2*$^{-/-}$;*Slc39a14*$^{-/-}$ mice was observed, but it did not reach statistical significance with this limited sample size ($n = 4$) (Figure 3D). Consistent with previous findings (Niederkofler et al., 2005), *Hfe2*$^{-/-}$ mice displayed reduced concentrations of iron in the spleen (Figure 3A), likely due to increased iron release by reticuloendothelial macrophages of the red pulp. Consequently, splenic accumulation of absorbed iron was markedly lower in *Hfe2*$^{-/-}$ mice compared to WT controls (Figure 3E). By contrast, splenic accumulation of absorbed iron was not lower in *Hfe2*$^{-/-}$;*Slc39a14*$^{-/-}$ mice (Figure 3E). Perls' stain of liver sections revealed massive iron deposition throughout hepatocytes of *Hfe2*$^{-/-}$ mice, but no iron deposits were detected in hepatocytes of *Hfe2*$^{-/-}$;*Slc39a14*$^{-/-}$ mice (Figures 3F and 3G). By using DAB-enhanced Perls' stain, however, iron deposits became detectable in nonparenchymal cells of the livers of *Hfe2*$^{-/-}$;*Slc39a14*$^{-/-}$ mice (Figure 3H). Costaining with the macrophage marker F4/80 and Perls' stain indicates that some, but not all, of the iron was present in Kupffer cells (Figure S3A). Loss of *Slc39a14* in the single- or double-knockout mice did not affect TIBC, transferrin saturation, or plasma NTBI concentrations (Figures 3J–3L). Mice lacking *Hfe2* had higher

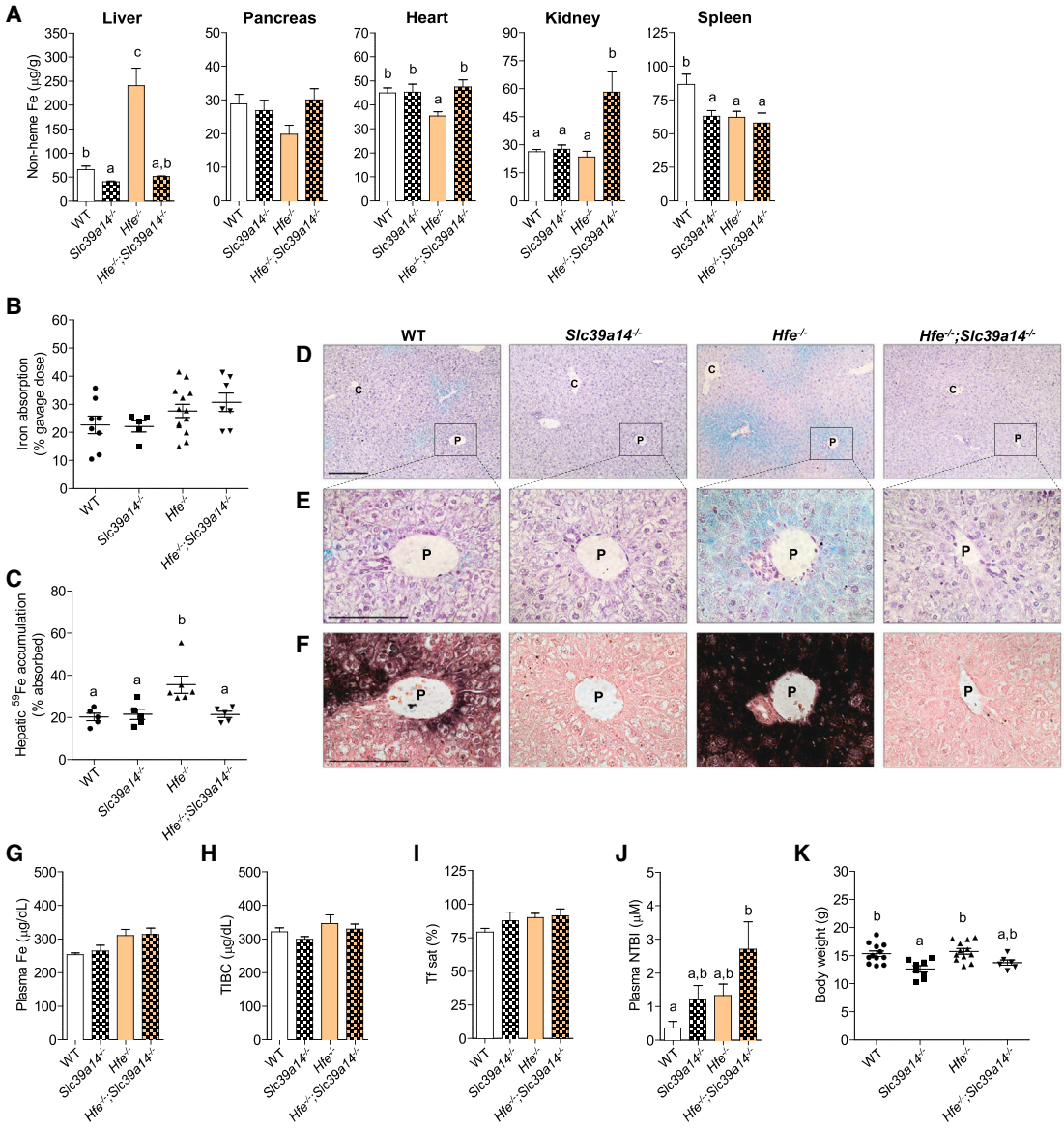

Figure 2. Ablation of *Slc39a14* in *Hfe*$^{-/-}$ Mice Impairs Hepatic Iron Loading

(A) Tissue nonheme iron concentrations in WT, *Slc39a14*$^{-/-}$, *Hfe*$^{-/-}$, and *Hfe*$^{-/-}$;*Slc39a14*$^{-/-}$ mice at 4 weeks of age (n = 5–9 per group).

(B) Iron absorption (% of dose) was measured after intragastric gavage of ^{59}Fe (n = 5–13 per group).

(C) Hepatic ^{59}Fe accumulation (percent of absorbed ^{59}Fe) was measured after intragastric gavage of ^{59}Fe (n = 5–6 per group).

(D–F) Representative images of Perls' iron stain in paraffin-embedded liver sections of mice at 4 weeks of age (n = 3 per group). Branches of the portal (P) and central (C) veins are indicated. (D and E) Liver sections processed by using standard Perls' iron stain (blue stain) and hematoxylin counterstain. Scale bars, 200 and 100 μm, respectively. (F) Serial liver sections processed by using DAB-enhanced Perls' stain (black stain) and neutral red counterstain. Scale bars, 100 μm.

(G–J) Plasma iron indices. (G) Plasma iron concentrations (n = 5–6 per group). (H) Total iron-binding capacity, TIBC (n = 5–6 per group). (I) Transferrin saturation (n = 5–6 per group). (J) Plasma NTBI concentrations (n = 8–13 per group).

(K) Body weights of mice at 4 weeks of age (n = 6–12 per group). All data are shown as the mean ± SEM. Means without a common superscript differ significantly ($p < 0.05$). See also Figure S1.

plasma NTBI concentrations relative to their respective controls (Figure 3L). Body weights were lower in *Hfe2*$^{-/-}$;*Slc39a14*$^{-/-}$ mice than in *Hfe2*$^{-/-}$ *and Slc39a14*$^{-/-}$ controls (Figure 3M). Older *Hfe2*$^{-/-}$; *Slc39a14*$^{-/-}$ mice (12 weeks of age) displayed alterations in tissue nonheme iron concentrations that were similar to those observed at 6 weeks of age (Figure S1E).

Loss of *Slc39a14* Alters Pancreatic Iron Accumulation

Given that the pancreas accumulates iron from NTBI (Craven et al., 1987) and that *Slc39a14*$^{-/-}$ mice showed impaired pancreatic NTBI uptake (Figure 1A), we expected that *Slc39a14*$^{-/-}$ mice would display impaired iron loading of this organ. Although we did find that pancreatic iron loading was

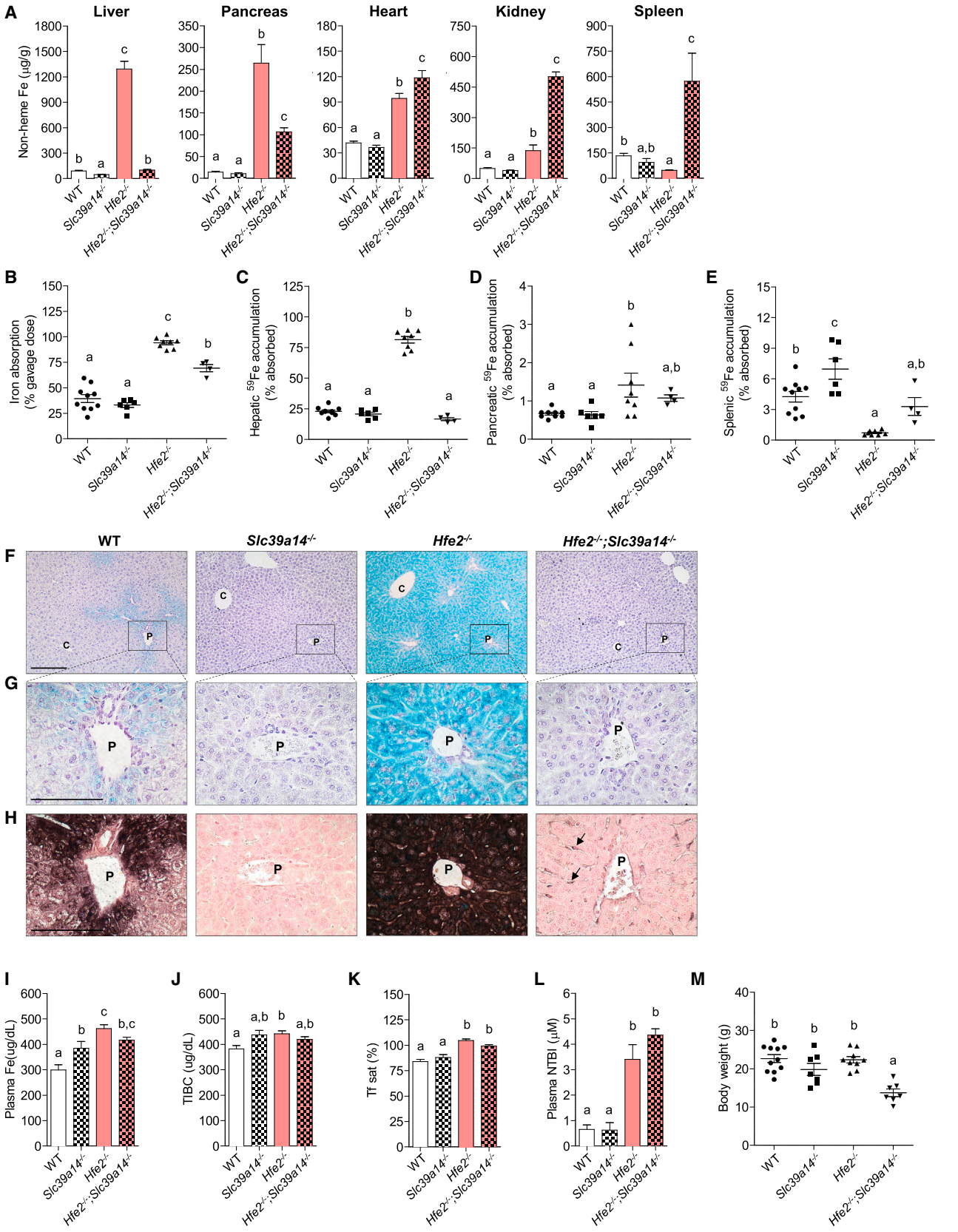

(legend on next page)

impaired in *Hfe2*$^{-/-}$;*Slc39a14*$^{-/-}$ mice relative to *Hfe2*$^{-/-}$ mice, iron still accumulated to levels that were roughly ten times normal (Figure 3A). In an effort to identify which cell types of the pancreas accumulated iron, we used DAB-enhanced Perls' stain, which was needed because Perls' stain was not sensitive enough to detect the low amounts of iron in this tissue at this age. Serial pancreas sections were counterstained with neutral red (+NR) to visualize tissue structures or processed without neutral red (−NR) to better see the iron deposits. Similar to a previous report (Niederkofler et al., 2005), *Hfe2*$^{-/-}$ mice accumulated iron predominantly in pancreatic acinar cells, with little iron detectable in islets (Figure 4A). However, in *Hfe2*$^{-/-}$;*Slc39a14*$^{-/-}$ mice, iron was not detected in acinar cells; instead, strong staining was observed in inter- and perilobular regions (Figure 4A). To identify which pancreatic structures were loading iron, we analyzed serial tissue sections by using immunohistochemistry and the protein markers PCK-26 for ductal epithelium, CD-31 for blood vessel endothelium, LYVE-1 for lymphatic endothelium, and collagen I for connective tissue. The iron staining overlapped best with collagen I (Figure 4B), suggesting that iron is depositing in connective tissue in the pancreas of *Hfe2*$^{-/-}$;*Slc39a14*$^{-/-}$ mice. Iron loading in pancreatic connective tissue has been reported previously (Giorgi and Roque, 2014). The altered pattern of pancreatic iron deposition in *Hfe2*$^{-/-}$;*Slc39a14*$^{-/-}$ mice is readily observed by Perls' staining of pancreas sections from 12-week-old mice (Figure S4A).

Loss of *Slc39a14* in Dietary Iron Overload

The data from the *Hfe*$^{-/-}$;*Slc39a14*$^{-/-}$ and *Hfe2*$^{-/-}$;*Slc39a14*$^{-/-}$ mice show that *Slc39a14* is required for the development of hepatic iron overload in mouse models of hemochromatosis. Given that the loss of *Hfe* and *Hfe2* results in hemochromatosis by impairing hepcidin expression, we next sought to examine what effect the loss of *Slc39a14* alone would have in the development of iron overload in mice having intact hepcidin regulation. To induce iron overload, WT and *Slc39a14*$^{-/-}$ mice were fed an iron-overloaded (FeO) diet for 4 weeks. Similar to the *Hfe*$^{-/-}$;*Slc39a14*$^{-/-}$ and *Hfe2*$^{-/-}$;*Slc39a14*$^{-/-}$ mice, *Slc39a14*$^{-/-}$ mice fed the FeO diet (*Slc39a14*$^{-/-}$-FeO mice) displayed a marked impairment in iron accumulation in the liver and increased iron loading in the pancreas, heart, kidney, and spleen (Figure 5A). Yet, unlike in the genetic models of iron overload, *Slc39a14*$^{-/-}$-FeO mice did accumulate a moderate amount of iron in the liver. However, Perls' stain of liver tissue sections from *Slc39a14*$^{-/-}$-FeO mice revealed a markedly altered cellular distribution of iron. In WT-FeO mice, iron predominantly accumulated in periportal hepatocytes (Figures 5B and 5C), whereas in *Slc39a14*$^{-/-}$-FeO mice, iron was found throughout the liver in nonparenchymal cells (Figures 5B and 5C), including Kupffer cells (Figure S3B). Magnification of a portal region from *Slc39a14*$^{-/-}$ mice revealed no detectable iron in hepatocytes (Figure 5C), even by using the highly sensitive DAB-enhanced Perls' stain (Figure 5D). DAB-enhanced Perls' stain of pancreas sections from *Slc39a14*$^{-/-}$-FeO mice revealed a pattern of iron deposition similar to that seen in *Hfe2*$^{-/-}$;*Slc39a14*$^{-/-}$ mice, i.e., iron staining in inter- and perilobular regions (Figure S4B). Plasma iron and NTBI concentrations did not differ among groups (Figures 5E and 5H), but transferrin saturations were higher in *Slc39a14*$^{-/-}$-FeO mice (Figure 5G), mainly because of lower TIBC (Figure 5F). Body weights of *Slc39a14*$^{-/-}$-FeO mice were lower than those of WT-FeO mice or *Slc39a14*$^{-/-}$-FeC mice (Figure 5I).

Loss of *Slc39a14* and Hepcidin Expression

Because the loss of *Slc39a14* impairs/alters hepatic iron accumulation in the three models of iron overload used in this study, we next asked whether these alterations would have an effect on hepatic expression of hepcidin, the iron-regulatory hormone produced mainly by the liver. We also measured hepatic mRNA levels of BMP6, a key endogenous regulator of hepcidin expression that is induced by hepatic iron loading (Kautz et al., 2008). Collectively, no differences in hepcidin mRNA levels were observed in *Slc39a14*$^{-/-}$ mice compared to their respective controls (Figures 6A–6C). Interestingly, however, BMP6 levels were elevated in iron-loaded *Slc39a14*$^{-/-}$ mice across all models used in the current study (Figures 6A–6C), despite these animals having markedly lower hepatic iron concentrations compared to their respective controls. For example, *Hfe2*$^{-/-}$ and *Hfe2*$^{-/-}$;*Slc39a14*$^{-/-}$ mice had similarly elevated BMP6 mRNA levels (i.e., 2.5-fold higher than WT or *Slc39a14*$^{-/-}$ mice) (Figure 6B), yet *Hfe2*$^{-/-}$;*Slc39a14*$^{-/-}$ mice had hepatic iron concentrations that were 12-fold lower than those in *Hfe2*$^{-/-}$ mice (i.e., 99 versus 1,292 mg Fe/g liver, Figure 3A). In *Slc39a14*$^{-/-}$-FeO mice, BMP6 mRNA levels were higher than those in WT-FeO mice (Figure 6C) despite these animals having 70% less iron in the liver (Figure 5A).

Although BMP6 is known to upregulate hepcidin expression, higher levels of BMP6 mRNA in *Slc39a14*$^{-/-}$-FeO mice compared with WT-FeO mice were not associated with further increases in hepcidin expression (Figure 6C). We initially thought that this result could be confounded by anemia, which we unexpectedly documented in a repeat study that we performed to obtain hemoglobin levels in the *Slc39a14*$^{-/-}$-FeO mice (Figure S5F). Anemia and associated stress erythropoiesis are known to cause the release of erythroid factors such as erythroferrone that suppress hepcidin expression (Kautz et al., 2014).

Figure 3. Ablation of *Slc39a14* in the *Hfe2*$^{-/-}$ Mouse Model of Juvenile Hemochromatosis Prevents Hepatic Iron Overload

(A) Tissue nonheme iron concentrations in WT, *Slc39a14*$^{-/-}$, *Hfe2*$^{-/-}$, and *Hfe2*$^{-/-}$;*Slc39a14*$^{-/-}$ mice at 6 weeks of age (n = 4–11 per group).

(B) Iron absorption (% of dose) was measured after intragastric gavage of ^{59}Fe (n = 4–10 per group).

(C–E) Hepatic, pancreatic, and splenic ^{59}Fe accumulation (percent of absorbed ^{59}Fe) was measured after intragastric gavage of ^{59}Fe (n = 4–11 per group).

(F–H) Representative images of Perls' iron stain in paraffin-embedded liver sections of mice at 6 weeks of age (n = 3 per group). (F and G) Liver sections processed by using standard Perls' iron stain (blue stain) and hematoxylin counterstain. Scale bars, 200 and 100 μm, respectively. (H) Serial liver sections processed by using DAB-enhanced Perls' stain (black stain) and neutral red counterstain. Arrows indicate iron deposits in nonparenchymal cells. Scale bars, 100 μm.

(I–L) Plasma iron indices. (I) Plasma iron concentrations (n = 4–6 per group). (J) Total iron-binding capacity, TIBC (n = 4–6 per group). (K) Transferrin saturation (n = 4–6 per group). (L) Plasma NTBI concentrations (n = 5–9 per group).

(M) Body weights of mice at 6 weeks of age (n = 7–11 per group). All data are shown as the mean ± SEM. Means without a common superscript differ significantly ($p < 0.05$). See also Figures S1–S3 and S5 and Table S1.

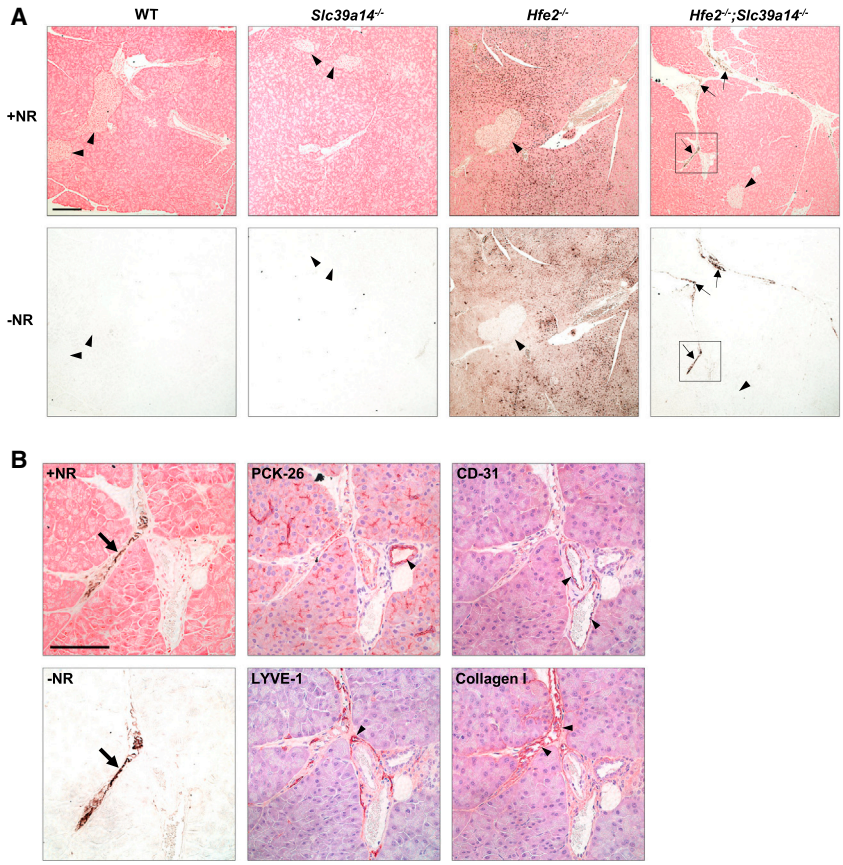

Figure 4. *Hfe2*$^{-/-}$;*Slc39a14*$^{-/-}$ Mice Display Altered Iron Loading in the Pancreas

(A) Representative images of DAB-enhanced Perls' iron stain in paraffin-embedded pancreas sections of WT, *Slc39a14*$^{-/-}$, *Hfe2*$^{-/-}$, and *Hfe2*$^{-/-}$;*Slc39a14*$^{-/-}$ mice at 6 weeks of age (n = 4 per group). Serial sections of pancreas processed in parallel by using DAB-enhanced Perls' iron stain (black stain) with or without neutral red counterstain (+NR and –NR, respectively). Black arrowheads indicate pancreatic islets. Arrows indicate iron deposits in *Hfe2*$^{-/-}$/*Slc39a14*$^{-/-}$ mice. Scale bar, 200 μm.

(B) Higher magnification of the boxed regions indicated in the *Hfe2*$^{-/-}$;*Slc39a14*$^{-/-}$ sections in (A) and representative images of serial sections from *Hfe2*$^{-/-}$;*Slc39a14*$^{-/-}$ mice showing immunostaining for markers of ductal epithelium (PCK-26), blood vessel endothelium (CD-31), lymphatic endothelium (LYVE-1), and connective tissue (collagen I), respectively (n = 4 per group). Slides processed for immunostaining were counterstained with hematoxylin. Arrows indicate iron deposits; arrowheads indicate areas of positive immunostaining (brown stain). Scale bar, 100 μm. See also Figure S4.

However, in a 3-day iron overload feeding study, which did not affect hemoglobin levels in the *Slc39a14*$^{-/-}$ mice, we again found elevated levels of BMP6 mRNA that were not associated with further increases in hepcidin expression (Figure S6). Our observations are similar to a dietary iron overload study in mice showing that increased BMP6 mRNA levels higher than 2-fold baseline are not associated with further increases in hepcidin mRNA (Corradini et al., 2011). Collectively, these observations suggest that BMP6 regulation of hepcidin expression becomes saturated at relatively low BMP6 expression levels. Nevertheless, additional studies are needed to determine if the unexpected hepcidin response in anemic *Slc39a14*$^{-/-}$-FeO mice is associated with erythropoiesis-driven factors that repress hepatic hepcidin production.

Loss of *Slc39a14* Alters Splenic Iron Accumulation

The accumulation of iron in the spleen in *Hfe2*$^{-/-}$;*Slc39a14*$^{-/-}$ mice (Figure 3A) was unexpected as these animals also expressed very low levels of hepcidin similar to *Hfe2*$^{-/-}$ mice (Figure 6B). Low hepcidin expression in *Hfe2*$^{-/-}$ mice is normally associated with decreased splenic iron concentrations, as observed in the present study (Figure 3A) and by others (Huang et al., 2005; Niederkofler et al., 2005). The lower splenic iron concentrations in *Hfe2*$^{-/-}$ mice are thought to arise from impaired hepcidin expression, which in turn fails to downregulate FPN expression in red pulp macrophages involved in recycling iron from senescent red blood cells. The elevated FPN levels and the resulting enhanced iron export in splenic macrophages therefore cause splenic iron levels to decrease. Our observation of splenic iron loading along with low hepcidin expression in *Hfe2*$^{-/-}$;*Slc39a14*$^{-/-}$ mice prompted us to examine the pattern of iron deposition and FPN expression in the spleen. Perls' staining of spleen sections from *Hfe2*$^{-/-}$;*Slc39a14*$^{-/-}$ mice revealed that iron accumulated in F4/80-positive macrophages of the red pulp (Figure S5A), with iron loading in cells expressing FPN (Figure S5B). One possible explanation for this observation is that when iron uptake by the liver and pancreas are impaired in iron-loaded *Hfe2*$^{-/-}$;*Slc39a14*$^{-/-}$ mice, NTBI in plasma is taken up by SLC39A14-independent mechanisms in splenic macrophages at a rate that exceeds the capacity of FPN to export the accumulated iron. Given that plasma NTBI concentrations did not differ between *Hfe2*$^{-/-}$ and *Hfe2*$^{-/-}$;*Slc39a14*$^{-/-}$ mice, it is also possible that the chemical composition of NTBI in *Hfe2*$^{-/-}$;*Slc39a14*$^{-/-}$ mice is different, favoring macrophage uptake. Selective uptake of different chemical forms of NTBI has been postulated to contribute to the different tissue iron loading patterns observed in various iron overload disorders (Arezes et al., 2013). More likely, however, the iron accumulation in red pulp macrophages of *Hfe2*$^{-/-}$;*Slc39a14*$^{-/-}$ mice is probably related to hemolysis, as suggested by lower hemoglobin levels, fewer total RBCs, normal MCV, and increased reticulocyte counts (Figure S5E; Table S1). Indeed, hemolysis may also be contributing to the anemia (Figure S5F; Table S2) and pronounced splenic iron accumulation in *Slc39a14*$^{-/-}$ mice subjected to dietary iron overload (Figures 5A and S5C).

DISCUSSION

In diseases of iron overload, the liver is the primary organ that accumulates iron, resulting in increased risk for hepatic fibrosis,

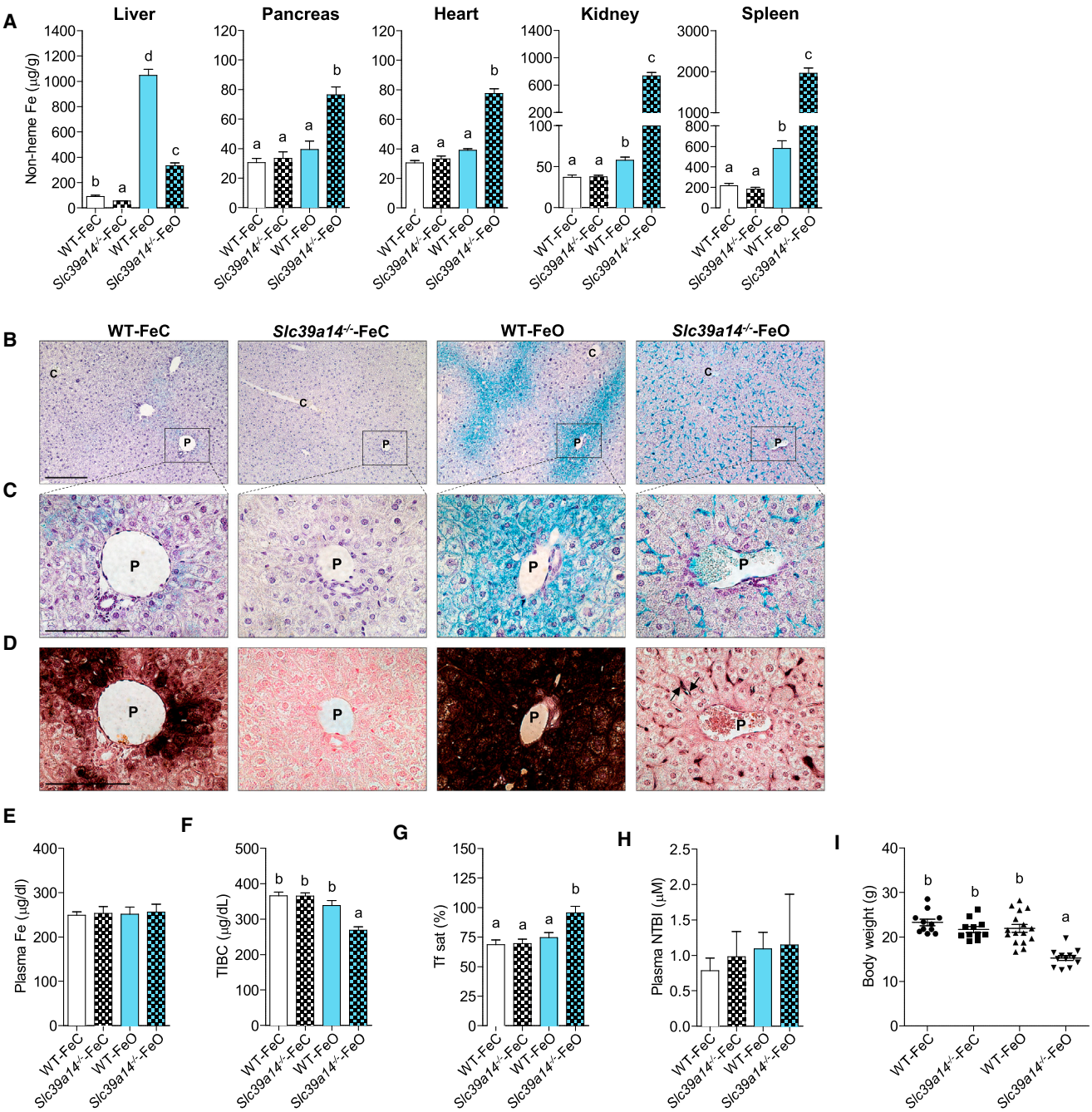

Figure 5. *Slc39a14*$^{-/-}$ Mice Display Altered Hepatic Iron Loading in Response to Dietary Iron Overload

(A) Tissue nonheme iron concentrations in weanling WT and *Slc39a14*$^{-/-}$ mice fed a normal-iron control diet (WT-FeC and *Slc39a14*$^{-/-}$-FeC) or an iron-overloaded diet (WT-FeO and *Slc39a14*$^{-/-}$-FeO) for 4 weeks (n = 6–10 per group). (B–D) Representative images of Perls' iron stain in paraffin-embedded liver sections of mice at 7 weeks of age (n = 3–4 per group). Branches of the portal (P) and central (C) veins are indicated.

(B and C) Liver sections processed by using standard Perls' iron stain (blue stain) and hematoxylin counterstain. Scale bars, 200 μm and 100 μm, respectively.

(D) Serial liver sections processed by using DAB-enhanced Perls' stain (black stain) and neutral red counterstain. Arrows indicate iron deposits in non-parenchymal cells. Scale bar, 100 μm.

(E–H) Plasma iron indices. (E) Plasma iron concentrations (n = 6–11 per group). (F) Total iron-binding capacity, TIBC (n = 6–11 per group). (G) Transferrin saturation (n = 6–11 per group). (H) Plasma NTBI concentrations (n = 5–6 per group).

(I) Body weights of mice at the end of the 4 week feeding study (n = 11–16 per group). All data are shown as the mean ± SEM. Means without a common superscript differ significantly ($p < 0.001$). See also Figures S4 and S5.

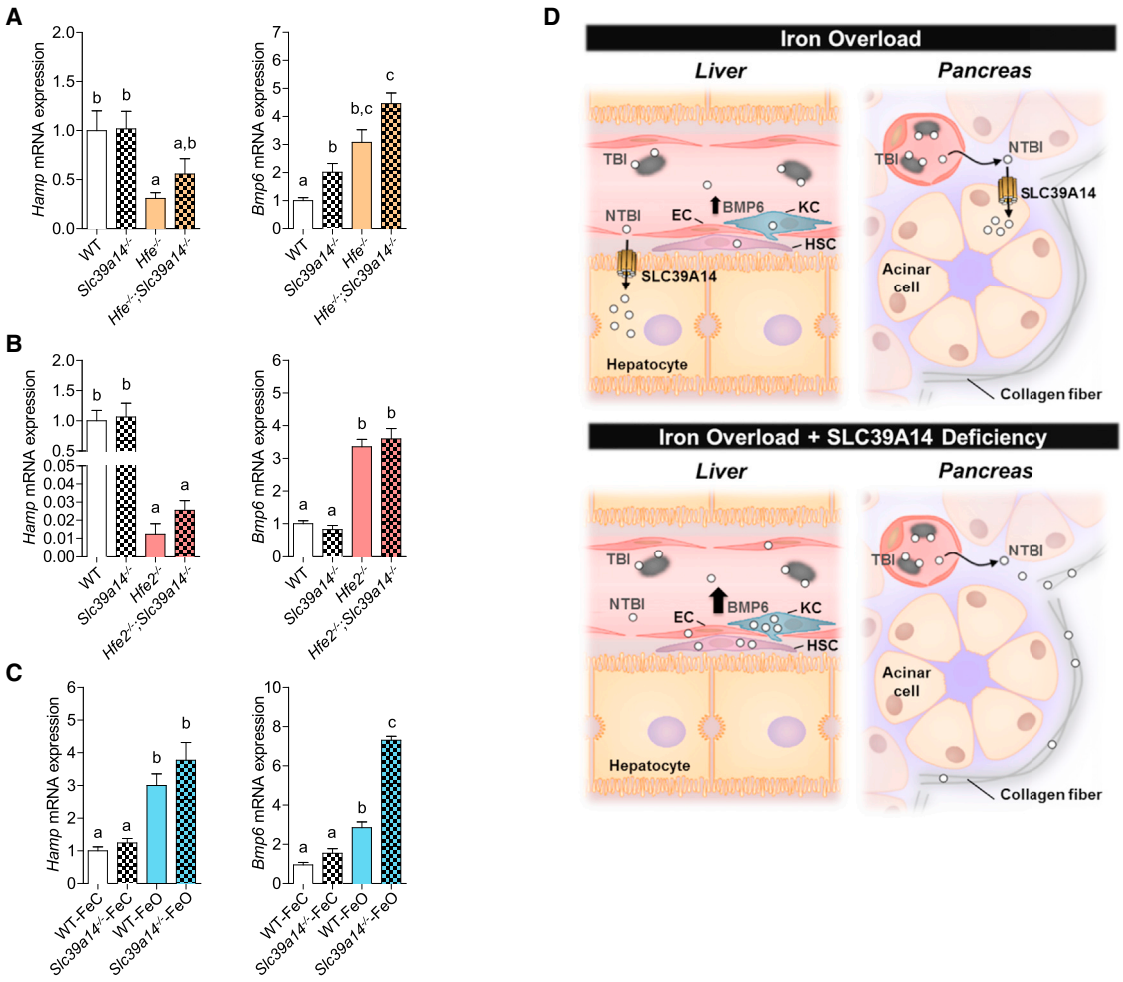

Figure 6. Hepatic Expression of *Hamp* and *Bmp6* mRNA in *Slc39a14*$^{-/-}$ Mice with Genetic or Dietary Iron Overload

(A–C) Relative expression of hepcidin (*Hamp*) and *Bmp6* mRNA was measured in (A) WT, *Slc39a14*$^{-/-}$, *Hfe*$^{-/-}$, and *Hfe*$^{-/-}$;*Slc39a14*$^{-/-}$ mice at 4 weeks of age (n = 7–9 per group); (B) WT, *Slc39a14*$^{-/-}$, *Hfe2*$^{-/-}$, and *Hfe2*$^{-/-}$;*Slc39a14*$^{-/-}$ mice at 6 weeks of age (n = 4–10 per group); and (C) WT-FeC, *Slc39a14*$^{-/-}$-FeC, WT-FeO and *Slc39a14*$^{-/-}$-FeO mice at 7 weeks of age (n = 6 per group). Transcript levels were normalized to those of *Rpl13a*. All data are shown as the mean ± SEM. Means without a common superscript differ significantly ($p < 0.01$).

(D) Proposed role of SLC39A14 in iron loading of the liver and pancreas and effect of SLC39A14 deficiency on hepatic BMP6 regulation. In iron overload, the iron-binding capacity of plasma transferrin (gray ovals) becomes exceeded, giving rise to NTBI, which loads into hepatocytes and pancreatic acinar cells via SLC39A14. In iron overload with SLC39A14 deficiency, iron does not load in hepatocytes or acinar cells but can accumulate in nonparenchymal cells of the liver (endothelial cells [ECs], hepatic stellate cells [HSCs], and Kupffer cells [KCs]) and collagen fibers in the pancreas. That hepatic BMP6 expression can be up-regulated in iron overload with SLC39A14 deficiency (A–C) suggests that BMP6 expression is regulated by SLC39A14-independent iron loading of non-parenchymal cells. See also Figure S6.

cirrhosis, and hepatocellular carcinoma (Pietrangelo, 2010). Yet, how the liver loads iron is largely unknown (Andrews, 2008; Wang and Knutson, 2013). Our present studies using double knockout *Hfe*$^{-/-}$;*Slc39a14*$^{-/-}$ and *Hfe2*$^{-/-}$;*Slc39a14*$^{-/-}$ mice reveal that *Slc39a14* is required for the development of hepatic iron overload in hereditary hemochromatosis. This is observed for both male and female mice, which are known to vary in iron status (Figures S1A and S1B). Furthermore, the observation that *Slc39a14*$^{-/-}$ mice displayed a marked impairment in the uptake of NTBI but not of TBI supports the hypothesis that NTBI is the main contributor to hepatic iron loading in iron overload disorders (Brissot et al., 2012).

Consistent with the double knockout mice, *Slc39a14*$^{-/-}$ mice subjected to dietary iron overload did not accumulate iron in hepatocytes; however, they did accumulate iron in hepatic macrophages (Kupffer cells), likely because these animals upregulated the expression of hepcidin, which blocks macrophage iron release (Knutson et al., 2005). Collectively, our genetic and dietary models of iron overload indicate that SLC39A14 is required for hepatocyte iron loading. Our data from *Hfe2*$^{-/-}$;*Slc39a14*$^{-/-}$ mice and dietary-iron-loaded *Slc39a14*$^{-/-}$ mice further suggest that SLC39A14 is required for iron loading of pancreatic acinar cells, the cell type of the pancreas that preferentially loads iron in hereditary hemochromatosis (Lesbordes-Brion et al., 2006; Nick et al., 2009).

Although SLC39A14 appears to be the main pathway for NTBI uptake by the liver and pancreas, our data indicate that SLC39A14 is dispensable for NTBI uptake and iron loading of

the heart. Cardiac iron accumulation can lead to iron-overload cardiomyopathy, estimated to account for one-third of deaths in hemochromatosis patients (Kremastinos and Farmakis, 2011). Our NTBI injection experiments indicate that the heart normally takes up very little plasma NTBI—in fact about 100 times less than the liver and 10 times less than the pancreas. These relative differences in NTBI uptake likely account for the observation that cardiac iron loading is usually a late manifestation of iron overload, occurring after the liver and pancreas become loaded with iron (Noetzli et al., 2009; Subramaniam et al., 2012). The finding that SLC39A14 is dispensable for cardiac NTBI uptake may be because SLC39A14 protein levels are markedly lower in the heart than in the pancreas or liver (Nam et al., 2013). Possible alternative NTBI transporters in the heart include L-type Ca^{2+} channels (Oudit et al., 2006), T-type Ca^{2+} channels (Kumfu et al., 2011), or SLC39A8, which is closely related to SLC39A14 (Wang et al., 2012).

Based on the data presented here, we propose the following model for NTBI uptake and tissue iron loading in hereditary hemochromatosis. In hemochromatosis, hepcidin levels are abnormally low, resulting in increased iron release from reticuloendothelial macrophages and increased intestinal iron absorption. The increased iron release into the circulation causes transferrin saturations to be high or fully saturated; therefore, most of the iron absorbed by the intestine or released from splenic macrophages will enter the portal circulation as NTBI. The liver efficiently takes up NTBI from portal blood via SLC39A14 located on the sinusoidal membrane of hepatocytes (Nam et al., 2013) (Figure 6D). SLC39A14-mediated NTBI uptake by hepatocytes largely explains why the liver is the first and foremost organ that accumulates iron in hereditary hemochromatosis. NTBI not taken up by the liver is subsequently taken up mostly by SLC39A14 expressed by pancreatic acinar cells (Figure 6D), and to a lesser extent by SLC39A14-independent NTBI transporters in the heart and other tissues. In hemochromatotic mice lacking SLC39A14, NTBI in portal blood bypasses the liver and is taken up mainly by the kidney, after being filtered through the glomeruli and reabsorbed in the proximal tubule by luminal transporters such as DMT1 or SLC39A8 (Canonne-Hergaux and Gros, 2002; Fujishiro et al., 2012).

The observation that hepatic hepcidin mRNA expression was unaffected by the loss of *Slc39a14*, either in single- or double-knockout mice, indicates that the markedly altered tissue distribution of iron in *Slc39a14*$^{-/-}$ mice does not arise because of altered expression of hepcidin, the master hormone that controls whole-body iron balance (Ganz and Nemeth, 2011). Our data additionally show that hepatic hepcidin mRNA, produced predominantly by hepatocytes, can be induced in the absence of detectable hepatocyte iron loading. In mice, hepcidin expression requires BMP6, a cytokine that triggers the BMP6/SMAD4-signaling pathway, ultimately activating hepcidin transcription (Andriopoulos et al., 2009; Meynard et al., 2009). Iron loading of the liver induces the expression of BMP6 (Kautz et al., 2008), which increases the expression of hepcidin. Although the hepatic cell type that increases BMP6 expression in response to iron loading remains unresolved, studies of isolated liver cells suggest that nonparenchymal cells (Kupffer cells, stellate cells, and sinusoidal endothelial cells) are the main source (Enns et al., 2013; Feng et al., 2012). Our data support this view in that upregulated BMP6 mRNA levels in iron-loaded *Slc39a14*$^{-/-}$ mice were associated with iron loading in nonparenchymal cells but not hepatocytes (Figure 6D).

In contrast to the dramatic alterations in iron metabolism observed in *Slc39a14*$^{-/-}$ mice with iron overload, only minor perturbations in iron metabolism were observed in normal *Slc39a14*$^{-/-}$ mice (i.e., single mutant *Slc39a14*$^{-/-}$ mice consuming diets with normal amounts of iron). One consistent finding was that liver nonheme iron concentrations were ~35% lower in young *Slc39a14*$^{-/-}$ mice compared with WT animals. This difference was observed at 4, 6, and 7 weeks of age (Figures 2A, 3A, and 5A, respectively). By 12–16 weeks, however, liver nonheme iron concentrations did not differ between groups (Figures S1D and S1E). We originally reported that liver iron levels were unaffected in normal *Slc39a14*$^{-/-}$ mice (Hojyo et al., 2011), but these data were from pool of mice of various ages (4, 8, and 16 weeks), as we later noted (Nam et al., 2013). A recent study reported that *Slc39a14*$^{-/-}$ mice had liver nonheme iron concentrations that were ~50% higher than WT mice (Beker Aydemir et al., 2012), but the age of the mice was not specified (only a range of 8–16 weeks was noted), and iron metabolism was not examined in the context of iron overload.

In conclusion, we identify SLC39A14 as the major route for NTBI uptake into hepatocytes and pancreatic acinar cells in iron overload and show that SLC39A14 is essential for iron loading of the liver in hereditary hemochromatosis. Our data raise the possibility that inhibitors of SLC39A14 activity or expression could be used to prevent hepatic iron loading in iron overload diseases, including transfusion-dependent thalassemia major, for which there is no cure at the present time. Such a strategy, however, would need to be used in conjunction with iron chelators that bind and remove NTBI from the plasma to prevent it from depositing in extrahepatic tissues.

EXPERIMENTAL PROCEDURES

Animals and Diets

Slc39a14$^{+/-}$ mice were originally on a mixed 129+Ter/SvJcl x C57BL/6 background (Hojyo et al., 2011). For tissue NTBI and TBI uptake measurements and the feeding study, *Slc39a14*$^{-/-}$ mice and wild-type (WT) control littermates were on a mixed 129+Ter/SvJcl × C57BL/6 × Balb/cJ background. For studies with double knockout mice, *Slc39a14*$^{+/-}$ mice were intercrossed with *Hfe*$^{+/-}$ mice (Levy et al., 1999) or *Hfe2*$^{+/-}$ mice (JAX Mice) on a 129S6/SvEvTac background to generate homozygous double knockout mice along with single mutant and WT littermate controls. Mice were genotyped at weaning by extracting genomic DNA from tail snip samples followed by PCR analysis. Mice were weaned at 3 weeks of age, maintained on a standard diet (Teklad 7912, Harlan Laboratories) containing 240 ppm iron, and housed in a 12 hr light-dark cycle. In the feeding study, mice were fed modified AIN-93G rodent diet formulated to contain 50 ppm iron (iron control, FeC; Harlan Laboratories, diet TD.130018) or 10,000 ppm (1%) carbonyl iron (iron overloaded, FeO; Harlan Laboratories, diet TD.130015) for 4 weeks. Mice in all studies were of mixed sex unless otherwise noted. The numbers of male and female mice used in all experiments are outlined in Tables S3 and S4. Animal protocols were approved by the Institutional Animal Care and Use Committee at the University of Florida.

Measurement of In Vivo Tissue NTBI and TBI Uptake

Tissue NTBI uptake was measured after intravenous administration of radiolabeled iron (Craven et al., 1987). Six-week-old mice were injected via tail vein with 70 μg ferric citrate in 0.1 ml of 0.1 M citric acid buffer (pH 6.6) to transiently saturate plasma transferrin. Ten minutes later, ^{59}Fe-labeled ferric-citrate

(2 μCi) was administered via tail vein. Mice were sacrificed 2 hr later, and whole-body and tissue ^{59}Fe-associated radioactivity (counts per min, cpm) were determined by using a WIZARD2 gamma counter (PerkinElmer). For tissue TBI uptake (Wang and Knutson, 2013), mice were injected via tail vein with 150 μg ^{59}Fe-labeled transferrin (2 μCi). Two hours later, animals were sacrificed and whole-body and tissue radioactivity were determined by gamma counting. NTBI and TBI uptakes were calculated as a percentage of whole-body cpm.

Primary Hepatocyte Isolation and Hepatocyte NTBI Uptake

Primary hepatocytes were isolated from 13-week-old mice by collagenase perfusion as detailed in Supplemental Information. Cellular uptake of NTBI (^{59}Fe-labeled ferric citrate) was measured as described previously (Wang et al., 2012) and as detailed in Supplemental Information.

Measurement of Iron Absorption

Iron absorption was determined by ^{59}Fe gavage (Ajioka et al., 2002). Five-week-old mice were fasted overnight and then gavaged with 0.2 ml ^{59}Fe-labeled iron solution containing ~2.5 μCi ^{59}Fe-HCl, 0.5 M ascorbic acid, 0.15 M NaCl, and $FeSO_4$ for a final total of 5 μg Fe. After gavage, mice were returned to their cages, provided with water, fasted for 7 hr, and then provided with food overnight. Approximately 24 hr after gavage, mice were sacrificed and dissected. The gastrointestinal (GI) tract was removed, and major organs and carcass were analyzed for radioactivity by gamma counting. Percentage iron absorption was calculated as (absorbed cpm/cpm of iron administered by gavage) × 100. Iron accumulation in various organs after ^{59}Fe gavage was calculated as organ cpm / absorbed cpm × 100. Absorbed cpm refers to the radioactivity in the whole body (determined by the sum of major organs and carcass cpm) without the GI tract.

Iron Status Parameters

Plasma iron, total iron-binding capacity, transferrin saturation, and tissue nonheme iron concentrations were determined as described previously (Wang and Knutson, 2013). Plasma NTBI was measured by using a colorimetric method (Gosriwatana et al., 1999). The distribution of storage iron in deparaffinized formalin-fixed tissues sections was visualized by using Perls' Prussian blue stain or diaminobenzidine (DAB)-enhanced Perls' stain containing cobalt chloride, which further enhances sensitivity and produces a black reaction product providing more contrast (Adams, 1981) as detailed in Supplemental Information. Slides were counterstained with 1% neutral red solution or hematoxylin QS (Vector Labs) and visualized with an Olympus IX70 inverted microscope and QImaging QCapture Pro 6.0 Software.

Immunoblot Analyses

Immunoblot analyses and sample preparation are detailed in Supplemental Information.

Immunohistochemistry

For immunohistochemical analysis, paraffin-embedded pancreas sections (except those for LYVE-1) were processed for antigen retrieval in sodium citrate buffer (pH 6.0). Slides were incubated for 30 min with primary antibody against PCK-26 (1:500; Abcam, ab6401), CD-31 (1:50; Abcam, ab28364), LYVE-1 (1:50; Abcam; ab14917), or collagen-I (1:100; NB600-408, Novus Biologicals). After incubation with species-specific biotinylated secondary antibodies (1:200) for 30 min and streptavidin-HRP for 30 min (Vectastain, ABC kit; Vector Labs), the immunoperoxidase reaction was visualized by using the VECTOR NovaRED Peroxidase HRP Substrate Kit (Vector Labs). Slides were counterstained with hematoxylin QS and visualized with an Olympus IX70 inverted microscope and QImaging QCapture Pro 6.0 Software.

RNA Extraction and Quantitative Reverse-Transcriptase PCR

Total RNA was isolated from liver samples by using RNAzol RT reagent (Molecular Research Center). First-strand cDNA synthesis was performed by using the High Capacity cDNA Reverse Transcriptase Kit (Applied Biosystems). PCR reactions were carried out by using the Power SYBR Green PCR kit (Applied Biosystems) on the ABI 7300 Real-Time PCR system (Applied Biosystems). Gene-specific primers used for PCR are listed in Supplemental Information.

Statistical Analyses

All data are shown as the mean ± SEM. Means were compared by using, where appropriate, Student's unpaired t test or one-way ANOVA with Tukey's post-hoc test. A p value <0.05 was considered statistically significant. Data sets with unequal variances were log transformed prior to statistical analysis. Analyses were performed by using PRISM software (GraphPad).

SUPPLEMENTAL INFORMATION

Supplemental Information includes six figures, four tables, and Supplemental Experimental Procedures and can be found with this article at http://dx.doi.org/10.1016/j.cmet.2015.05.002.

AUTHOR CONTRIBUTIONS

M.D.K., S.J., and C.-Y.W. designed the experiments and analyzed the data. M.D.K., S.J., T.F., and S.H. wrote the manuscript. S.J., C.-Y.W., R.C., and W.Z. performed the mouse experiments, iron analyses, and immunohistochemistry. A.C. assisted with mouse breeding and genotyping. T.B. and J.-S.K. isolated primary mouse hepatocytes. S.H. and T.F. provided the *Slc39a14*$^{-/-}$ mice.

ACKNOWLEDGMENTS

This work was supported by the National Institutes of Health grant DK080706 (to M.D.K.) and grants DK079879 and DK090115 (to J.-S.K.), and by the National Institute on Aging grant AG028740 (J.-S.K.). We thank Martha Campbell-Thompson (Department of Medicine, University of Florida) for help with anatomy and immunohistochemistry of the pancreas, and Dr. Herbert Y. Lin (Harvard Medical School, Boston, MA) for assistance with studies on *Hfe2*$^{-/-}$ mice.

Received: September 3, 2014
Revised: March 4, 2015
Accepted: April 24, 2015
Published: May 28, 2015

REFERENCES

Adams, J.C. (1981). Heavy metal intensification of DAB-based HRP reaction product. J. Histochem. Cytochem. *29*, 775.

Ajioka, R.S., Levy, J.E., Andrews, N.C., and Kushner, J.P. (2002). Regulation of iron absorption in Hfe mutant mice. Blood *100*, 1465–1469.

Andrews, N.C. (2008). Forging a field: the golden age of iron biology. Blood *112*, 219–230.

Andriopoulos, B., Jr., Corradini, E., Xia, Y., Faasse, S.A., Chen, S., Grgurevic, L., Knutson, M.D., Pietrangelo, A., Vukicevic, S., Lin, H.Y., and Babitt, J.L. (2009). BMP6 is a key endogenous regulator of hepcidin expression and iron metabolism. Nat. Genet. *41*, 482–487.

Arezes, J., Costa, M., Vieira, I., Dias, V., Kong, X.L., Fernandes, R., Vos, M., Carlsson, A., Rikers, Y., Porto, G., et al. (2013). Non-transferrin-bound iron (NTBI) uptake by T lymphocytes: evidence for the selective acquisition of oligomeric ferric citrate species. PLoS ONE *8*, e79870.

Beker Aydemir, T., Chang, S.M., Guthrie, G.J., Maki, A.B., Ryu, M.S., Karabiyik, A., and Cousins, R.J. (2012). Zinc transporter ZIP14 functions in hepatic zinc, iron and glucose homeostasis during the innate immune response (endotoxemia). PLoS ONE *7*, e48679.

Bradbury, M.W., Raja, K., and Ueda, F. (1994). Contrasting uptakes of 59Fe into spleen, liver, kidney and some other soft tissues in normal and hypotransferrinaemic mice. Influence of an antibody against the transferrin receptor. Biochem. Pharmacol. *47*, 969–974.

Bridle, K.R., Frazer, D.M., Wilkins, S.J., Dixon, J.L., Purdie, D.M., Crawford, D.H., Subramaniam, V.N., Powell, L.W., Anderson, G.J., and Ramm, G.A. (2003). Disrupted hepcidin regulation in HFE-associated haemochromatosis and the liver as a regulator of body iron homoeostasis. Lancet *361*, 669–673.

Brissot, P., Ropert, M., Le Lan, C., and Loréal, O. (2012). Non-transferrin bound iron: a key role in iron overload and iron toxicity. Biochim. Biophys. Acta *1820*, 403–410.

Cabantchik, Z.I. (2014). Labile iron in cells and body fluids: physiology, pathology, and pharmacology. Front. Pharmacol. *5*, 45.

Camaschella, C., Roetto, A., Calì, A., De Gobbi, M., Garozzo, G., Carella, M., Majorano, N., Totaro, A., and Gasparini, P. (2000). The gene TFR2 is mutated in a new type of haemochromatosis mapping to 7q22. Nat. Genet. *25*, 14–15.

Canonne-Hergaux, F., and Gros, P. (2002). Expression of the iron transporter DMT1 in kidney from normal and anemic mk mice. Kidney Int. *62*, 147–156.

Carpenter, J.P., Grasso, A.E., Porter, J.B., Shah, F., Dooley, J., and Pennell, D.J. (2013). On myocardial siderosis and left ventricular dysfunction in hemochromatosis. J. Cardiovasc. Magn. Reson. *15*, 24.

Corradini, E., Meynard, D., Wu, Q., Chen, S., Ventura, P., Pietrangelo, A., and Babitt, J.L. (2011). Serum and liver iron differently regulate the bone morphogenetic protein 6 (BMP6)-SMAD signaling pathway in mice. Hepatology *54*, 273–284.

Craven, C.M., Alexander, J., Eldridge, M., Kushner, J.P., Bernstein, S., and Kaplan, J. (1987). Tissue distribution and clearance kinetics of non-transferrin-bound iron in the hypotransferrinemic mouse: a rodent model for hemochromatosis. Proc. Natl. Acad. Sci. USA *84*, 3457–3461.

Enns, C.A., Ahmed, R., Wang, J., Ueno, A., Worthen, C., Tsukamoto, H., and Zhang, A.S. (2013). Increased iron loading induces Bmp6 expression in the non-parenchymal cells of the liver independent of the BMP-signaling pathway. PLoS ONE *8*, e60534.

Feder, J.N., Gnirke, A., Thomas, W., Tsuchihashi, Z., Ruddy, D.A., Basava, A., Dormishian, F., Domingo, R., Jr., Ellis, M.C., Fullan, A., et al. (1996). A novel MHC class I-like gene is mutated in patients with hereditary haemochromatosis. Nat. Genet. *13*, 399–408.

Feng, Q., Migas, M.C., Waheed, A., Britton, R.S., and Fleming, R.E. (2012). Ferritin upregulates hepatic expression of bone morphogenetic protein 6 and hepcidin in mice. Am. J. Physiol. Gastrointest. Liver Physiol. *302*, G1397–G1404.

Fleming, R.E., Holden, C.C., Tomatsu, S., Waheed, A., Brunt, E.M., Britton, R.S., Bacon, B.R., Roopenian, D.C., and Sly, W.S. (2001). Mouse strain differences determine severity of iron accumulation in Hfe knockout model of hereditary hemochromatosis. Proc. Natl. Acad. Sci. USA *98*, 2707–2711.

Fleming, R.E., Britton, R.S., Waheed, A., Sly, W.S., and Bacon, B.R. (2005). Pathophysiology of hereditary hemochromatosis. Semin. Liver Dis. *25*, 411–419.

Fujishiro, H., Yano, Y., Takada, Y., Tanihara, M., and Himeno, S. (2012). Roles of ZIP8, ZIP14, and DMT1 in transport of cadmium and manganese in mouse kidney proximal tubule cells. Metallomics *4*, 700–708.

Ganz, T., and Nemeth, E. (2011). Hepcidin and disorders of iron metabolism. Annu. Rev. Med. *62*, 347–360.

Gao, J., Zhao, N., Knutson, M.D., and Enns, C.A. (2008). The hereditary hemochromatosis protein, HFE, inhibits iron uptake via down-regulation of Zip14 in HepG2 cells. J. Biol. Chem. *283*, 21462–21468.

Giorgi, G., and Roque, M.E. (2014). Iron overload induces changes of pancreatic and duodenal divalent metal transporter 1 and prohepcidin expression in mice. Acta Histochem. *116*, 354–362.

Gosriwatana, I., Loreal, O., Lu, S., Brissot, P., Porter, J., and Hider, R.C. (1999). Quantification of non-transferrin-bound iron in the presence of unsaturated transferrin. Anal. Biochem. *273*, 212–220.

Gunshin, H., Fujiwara, Y., Custodio, A.O., Direnzo, C., Robine, S., and Andrews, N.C. (2005). Slc11a2 is required for intestinal iron absorption and erythropoiesis but dispensable in placenta and liver. J. Clin. Invest. *115*, 1258–1266.

Hershko, C., Graham, G., Bates, G.W., and Rachmilewitz, E.A. (1978). Non-specific serum iron in thalassaemia: an abnormal serum iron fraction of potential toxicity. Br. J. Haematol. *40*, 255–263.

Hojyo, S., Fukada, T., Shimoda, S., Ohashi, W., Bin, B.H., Koseki, H., and Hirano, T. (2011). The zinc transporter SLC39A14/ZIP14 controls G-protein coupled receptor-mediated signaling required for systemic growth. PLoS ONE *6*, e18059.

Huang, F.W., Pinkus, J.L., Pinkus, G.S., Fleming, M.D., and Andrews, N.C. (2005). A mouse model of juvenile hemochromatosis. J. Clin. Invest. *115*, 2187–2191.

Kautz, L., Meynard, D., Monnier, A., Darnaud, V., Bouvet, R., Wang, R.H., Deng, C., Vaulont, S., Mosser, J., Coppin, H., and Roth, M.P. (2008). Iron regulates phosphorylation of Smad1/5/8 and gene expression of Bmp6, Smad7, Id1, and Atoh8 in the mouse liver. Blood *112*, 1503–1509.

Kautz, L., Jung, G., Valore, E.V., Rivella, S., Nemeth, E., and Ganz, T. (2014). Identification of erythroferrone as an erythroid regulator of iron metabolism. Nat. Genet. *46*, 678–684.

Knutson, M., and Wessling-Resnick, M. (2003). Iron metabolism in the reticuloendothelial system. Crit. Rev. Biochem. Mol. Biol. *38*, 61–88.

Knutson, M.D., Oukka, M., Koss, L.M., Aydemir, F., and Wessling-Resnick, M. (2005). Iron release from macrophages after erythrophagocytosis is up-regulated by ferroportin 1 overexpression and down-regulated by hepcidin. Proc. Natl. Acad. Sci. USA *102*, 1324–1328.

Kremastinos, D.T., and Farmakis, D. (2011). Iron overload cardiomyopathy in clinical practice. Circulation *124*, 2253–2263.

Kumfu, S., Chattipakorn, S., Srichairatanakool, S., Settakorn, J., Fucharoen, S., and Chattipakorn, N. (2011). T-type calcium channel as a portal of iron uptake into cardiomyocytes of beta-thalassemic mice. Eur. J. Haematol. *86*, 156–166.

Le Lan, C., Loréal, O., Cohen, T., Ropert, M., Glickstein, H., Lainé, F., Pouchard, M., Deugnier, Y., Le Treut, A., Breuer, W., et al. (2005). Redox active plasma iron in C282Y/C282Y hemochromatosis. Blood *105*, 4527–4531.

Lesbordes-Brion, J.C., Viatte, L., Bennoun, M., Lou, D.Q., Ramey, G., Houbron, C., Hamard, G., Kahn, A., and Vaulont, S. (2006). Targeted disruption of the hepcidin 1 gene results in severe hemochromatosis. Blood *108*, 1402–1405.

Levy, J.E., Montross, L.K., Cohen, D.E., Fleming, M.D., and Andrews, N.C. (1999). The C282Y mutation causing hereditary hemochromatosis does not produce a null allele. Blood *94*, 9–11.

Liuzzi, J.P., Aydemir, F., Nam, H., Knutson, M.D., and Cousins, R.J. (2006). Zip14 (Slc39a14) mediates non-transferrin-bound iron uptake into cells. Proc. Natl. Acad. Sci. USA *103*, 13612–13617.

Merryweather-Clarke, A.T., Pointon, J.J., Shearman, J.D., and Robson, K.J. (1997). Global prevalence of putative haemochromatosis mutations. J. Med. Genet. *34*, 275–278.

Meynard, D., Kautz, L., Darnaud, V., Canonne-Hergaux, F., Coppin, H., and Roth, M.P. (2009). Lack of the bone morphogenetic protein BMP6 induces massive iron overload. Nat. Genet. *41*, 478–481.

Nam, H., Wang, C.Y., Zhang, L., Zhang, W., Hojyo, S., Fukada, T., and Knutson, M.D. (2013). ZIP14 and DMT1 in the liver, pancreas, and heart are differentially regulated by iron deficiency and overload: implications for tissue iron uptake in iron-related disorders. Haematologica *98*, 1049–1057.

Nick, H., Allegrini, P.R., Fozard, L., Junker, U., Rojkjaer, L., Salie, R., Niederkofler, V., and O'Reilly, T. (2009). Deferasirox reduces iron overload in a murine model of juvenile hemochromatosis. Exp. Biol. Med. (Maywood) *234*, 492–503.

Niederkofler, V., Salie, R., and Arber, S. (2005). Hemojuvelin is essential for dietary iron sensing, and its mutation leads to severe iron overload. J. Clin. Invest. *115*, 2180–2186.

Noetzli, L.J., Papudesi, J., Coates, T.D., and Wood, J.C. (2009). Pancreatic iron loading predicts cardiac iron loading in thalassemia major. Blood *114*, 4021–4026.

Nomura, N., Nagase, T., Miyajima, N., Sazuka, T., Tanaka, A., Sato, S., Seki, N., Kawarabayasi, Y., Ishikawa, K., and Tabata, S. (1994). Prediction of the coding sequences of unidentified human genes. II. The coding sequences of 40 new genes (KIAA0041-KIAA0080) deduced by analysis of cDNA clones from human cell line KG-1. DNA Res. *1*, 223–229.

Oudit, G.Y., Trivieri, M.G., Khaper, N., Liu, P.P., and Backx, P.H. (2006). Role of L-type Ca2+ channels in iron transport and iron-overload cardiomyopathy. J. Mol. Med. *84*, 349–364.

Papanikolaou, G., Samuels, M.E., Ludwig, E.H., MacDonald, M.L., Franchini, P.L., Dubé, M.P., Andres, L., MacFarlane, J., Sakellaropoulos, N., Politou, M., et al. (2004). Mutations in HFE2 cause iron overload in chromosome 1q-linked juvenile hemochromatosis. Nat. Genet. *36*, 77–82.

Pietrangelo, A. (2010). Hereditary hemochromatosis: pathogenesis, diagnosis, and treatment. Gastroenterology *139*, 393–408, e1–e2.

Pinilla-Tenas, J.J., Sparkman, B.K., Shawki, A., Illing, A.C., Mitchell, C.J., Zhao, N., Liuzzi, J.P., Cousins, R.J., Knutson, M.D., and Mackenzie, B. (2011). Zip14 is a complex broad-scope metal-ion transporter whose functional properties support roles in the cellular uptake of zinc and nontransferrin-bound iron. Am. J. Physiol. Cell Physiol. *301*, C862–C871.

Rahier, J., Loozen, S., Goebbels, R.M., and Abrahem, M. (1987). The haemochromatotic human pancreas: a quantitative immunohistochemical and ultrastructural study. Diabetologia *30*, 5–12.

Roetto, A., Papanikolaou, G., Politou, M., Alberti, F., Girelli, D., Christakis, J., Loukopoulos, D., and Camaschella, C. (2003). Mutant antimicrobial peptide hepcidin is associated with severe juvenile hemochromatosis. Nat. Genet. *33*, 21–22.

Subramaniam, V.N., McDonald, C.J., Ostini, L., Lusby, P.E., Wockner, L.F., Ramm, G.A., and Wallace, D.F. (2012). Hepatic iron deposition does not predict extrahepatic iron loading in mouse models of hereditary hemochromatosis. Am. J. Pathol. *181*, 1173–1179.

Taylor, K.M., Morgan, H.E., Johnson, A., and Nicholson, R.I. (2005). Structure-function analysis of a novel member of the LIV-1 subfamily of zinc transporters, ZIP14. FEBS Lett. *579*, 427–432.

Trinder, D., and Morgan, E. (1997). Inhibition of uptake of transferrin-bound iron by human hepatoma cells by nontransferrin-bound iron. Hepatology *26*, 691–698.

Wang, C.Y., and Knutson, M.D. (2013). Hepatocyte divalent metal-ion transporter-1 is dispensable for hepatic iron accumulation and non-transferrin-bound iron uptake in mice. Hepatology *58*, 788–798.

Wang, C.Y., Jenkitkasemwong, S., Duarte, S., Sparkman, B.K., Shawki, A., Mackenzie, B., and Knutson, M.D. (2012). ZIP8 is an iron and zinc transporter whose cell-surface expression is up-regulated by cellular iron loading. J. Biol. Chem. *287*, 34032–34043.

Zhao, N., Gao, J., Enns, C.A., and Knutson, M.D. (2010). ZRT/IRT-like protein 14 (ZIP14) promotes the cellular assimilation of iron from transferrin. J. Biol. Chem. *285*, 32141–32150.

Zhou, X.Y., Tomatsu, S., Fleming, R.E., Parkkila, S., Waheed, A., Jiang, J., Fei, Y., Brunt, E.M., Ruddy, D.A., Prass, C.E., et al. (1998). HFE gene knockout produces mouse model of hereditary hemochromatosis. Proc. Natl. Acad. Sci. USA *95*, 2492–2497.